

PAPER • OPEN ACCESS

Optimizing energy density in dielectric elastomer generators: a reliability-dependent metric

To cite this article: Emmanuel Taine *et al* 2024 *Smart Mater. Struct.* **33** 115030

View the [article online](#) for updates and enhancements.

You may also like

- [Hybrid piezoelectric–electrostatic generators for wearable energy harvesting applications](#)
Clara Lagomarsini, Claire Jean-Mistral, Giulia Lombardi et al.
- [Resonant wave energy harvester based on dielectric elastomer generator](#)
Giacomo Moretti, Gastone Pietro Rosati Papini, Michele Righi et al.
- [Temperature effect on the performance of a dissipative dielectric elastomer generator with failure modes](#)
S E Chen, L Deng, Z C He et al.



 The Electrochemical Society
Advancing solid state & electrochemical science & technology

247th ECS Meeting
Montréal, Canada
May 18-22, 2025
Palais des Congrès de Montréal

Showcase your science!

Abstract submission deadline extended: December 20

ECS UNITED

Optimizing energy density in dielectric elastomer generators: a reliability-dependent metric

Emmanuel Taine^{1,2,*} , Thomas Andritsch¹ , Istebreq A Saeedi¹ and Peter H F Morshuis³

¹ The Tony Davies High Voltage Laboratory, University of Southampton, Southampton, United Kingdom

² Research & Development Laboratory, SBM Offshore, Le Broc, France

³ Solid Dielectric Solutions, Leiden, The Netherlands

E-mail: et7n21@soton.ac.uk

Received 6 June 2024, revised 26 September 2024

Accepted for publication 7 October 2024

Published 17 October 2024



CrossMark

Abstract

Dielectric elastomer generators (DEGs) are soft transducers capable of converting mechanical energy into electrostatic energy. Increasing the mechanical stretch amplitude and the electric field imposed to the DEG leads to higher energy conversion at the cost of a reduced lifetime. Here, mechanical fatigue and electrical degradation were assessed on a silicone-based DEG, and the outcome was used to build an electro-mechanical reliability model. A novel metric, termed *levelized energy density*, has been introduced to carefully balance the conflicting objectives of high energy output and long-term reliability. Through a multi-dimensional analysis of this index, the optimal operating parameters (stretch amplitude and electric field) that maximize energy conversion can be derived. Energy densities reported in literature are generally obtained after pushing the DEG close to their intrinsic limits for a limited number of cycles. In our approach, more realistic values in the endurance domain are presented, which typically leads to a 9-fold decrease in energy density for a design life of 1 million cycles. This article not only addresses the challenge of optimizing DEG performance but also emphasizes the importance of considering realistic operational conditions to enhance reliability, ultimately contributing to the practical and sustainable deployment of these soft transducers in various applications.

Keywords: dielectric elastomer generator, electro-mechanical reliability, mechanical fatigue, electrical ageing, energy density

1. Introduction

Dielectric elastomer Generators (DEGs) offer a versatile platform for converting mechanical energy into electrostatic energy and hold promise for various applications from wearables to large scale energy harvesting. Energy densities higher

than $1 \text{ J}\cdot\text{g}^{-1}$ are theoretically achievable with DEGs [1–3], and the largest experimental energy density was obtained with an acrylic elastomer reaching $0.78 \text{ J}\cdot\text{g}^{-1}$ [4]. A decade later, this record still holds, demonstrating a certain limitation in the achievable conversion. Moreover, these attractive numbers might appear unachievable for long lasting devices as they were obtained from materials operated close to their intrinsic limits (namely the dielectric breakdown strength (DBS) and the strain at break) for a very limited number of cycles. In practical or commercial applications, the transducer will have to be operated well away from its critical points in the interest of reliability [5, 6] and, the largest energy density reported in the high-cycle domain is $0.1 \text{ J}\cdot\text{g}^{-1}$ after a continuous operation for more than 10^7 cycles [7]. Although the stretch amplitude

* Author to whom any correspondence should be addressed.



Original content from this work may be used under the terms of the [Creative Commons Attribution 4.0 licence](https://creativecommons.org/licenses/by/4.0/). Any further distribution of this work must maintain attribution to the author(s) and the title of the work, journal citation and DOI.

and the maximal electric field are the operating parameters which drive the energy conversion, maximizing these values can also induce fatigue failure or electrical breakdown with the consequence of a reduced lifetime. From an engineering perspective, a trade-off needs to be made between energy conversion and long-term reliability, which is usually based on the experience and good judgement of the operator. As an example, maximal operating electric field can range from 30% to 80% of the ultimate material limit [5, 8, 9] and with these points in view, a methodology is needed to determine the optimal settings. A similar arbitration applies to the operating stretch conditions. Zhou *et al* have introduced a first theoretical analysis concluding that mechanical fatigue could result in a lower efficiency of a DEG [10]. In 2018, the same authors have proposed a fatigue predictor for dielectric viscoelastomers which can provide guidelines for loading conditions of these materials [11]. Later, Jean-Mistral *et al* have introduced a metric which aims at evaluating the performance of a DEG from the entire energy converted U_c before reaching an electrical or mechanical failure [12]. This performance index is the product of the energy density w_e and cycles to failure N_f as defined by (1). It basically represents the total amount of energy converted over the material's lifetime and provides a useful ranking parameter to compare the performance of various elastomer formulations [13]

$$U_c = w_e N_f. \quad (1)$$

However, in the aforementioned studies, the reliability of the transducer was not considered in the overall energy balance. As an example, it is of interest to understand whether a system should rather be designed to respond to large and energetic stretch amplitudes with the risk of premature fatigue failure, or whether lower cycling amplitudes would ultimately exceed the total energy converted when the entire life of a system is considered. The same question applies to the electric field value applied to the dielectric which aims to be maximized from an energy standpoint with an enhanced risk of electrical breakdown from a reliability standpoint. In this study, a reliability dependent metric was introduced which allows to answer these seemingly straightforward questions.

In the first part of this paper, the electrical and mechanical reliabilities of a silicone-based DEG were experimentally evaluated, which allowed us to propose an electro-mechanical reliability model. Its output was introduced into a modified version of the performance index introduced in (1), where both the energetic consideration and stochastic nature of failures are considered. Then, a parametric study allows the determination of the stretch and electric field (denoted λ and E respectively) which maximize the total energy converted over the DEG lifetime. The resulting operating parameters can be used as design guidelines and the outcome gives more comprehensive energy density values for long-lasting devices (as opposed to the energy density resulting from the intrinsic material limits).

2. Background

2.1. Energy conversion

When the DEG is stretched by an external work, its electrical capacitance (2) increases by the combined effect of surface expansion and thickness reduction, with ε the permittivity of the dielectric elastomer, A the active area covered by electrodes, and d the thickness of the dielectric layer. The obtained time-varying capacitance can be used to raise charges from a low to a high voltage resulting in a gain in electrostatic energy

$$C = \varepsilon A/d. \quad (2)$$

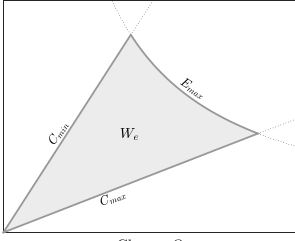
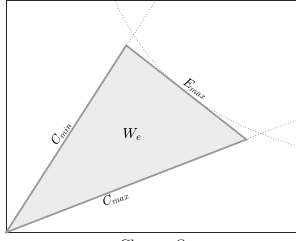
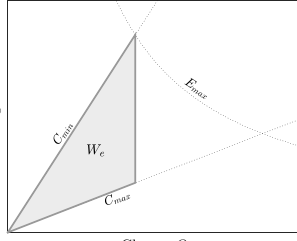
The maximal energy conversion can be obtained from what is known as the constant electric field (CE) cycle, where the voltage level V is adjusted according to the variation of thickness in the relaxing phase to maintain a constant maximal electric field E_{\max} in the dielectric elastomer. While the CE scheme offers the highest energy conversion, its widespread adoption is hindered by the need for sophisticated electronics. In addition, this study investigates two simpler alternative conversion methods: the optimal triangle cycle (OT) and the constant charge cycle (CC). The net energy converted W_e is graphically represented as the area of the hysteric loop in a charge-voltage ($Q - V$) plane bounded between the two iso-capacitance lines and the maximal electric field line (table 1). The energy density w_e corresponds to the net energy converted per cycle and per mass unit of dielectric elastomer. Assuming negligible viscoelastic and dielectric losses, table 1 provides equations for w_e for each scheme, with β the capacitance swing (which is defined as the ratio of maximal to minimal capacitance $\beta = C_{\max}/C_{\min}$) and ρ the mass density of the dielectric [6].

2.2. Electrical limits

The DBS is the ultimate physical limits which drives the electric performance of a dielectric elastomers. Determining the DBS of a given material and its underlying failure mechanisms is of primary importance for defining a safe operational voltage. In literature, a number of parameters are found to influence the electrical limits of dielectric elastomers. Among them, elastomer stiffness [14, 15] or amount of pre-stretch [16, 17] can determine the onset of electromechanical instabilities which is acknowledged as the major electrical failure mechanism for dielectric elastomers. This electrical failure mechanism is particularly relevant for the harvesting schemes presented in table 1 as the electric field is high when the elastomer is at its minimal stretch.

The mechanical damage resulting from both the Mullins effect and cycle softening is also found to modify the critical instability leading to lower breakdown values after mechanical

Table 1. Energy conversion in a charge–voltage plane and energy densities of the different cycles [6].

Cycle	CE	OT	CC
$Q - V$ plane			
w_e	$\frac{\varepsilon E_{\max}^2 \ln(\sqrt{\beta})}{\rho}$	$\frac{2\varepsilon E_{\max}^2 (\sqrt{\beta}-1)}{\rho(\sqrt{\beta}+1)}$	$\frac{\varepsilon E_{\max}^2}{2\rho} \left(1 - \frac{1}{\beta}\right)$

cycling [18]. In full-scale equipment, defects that are inevitably introduced in the manufacturing process are the limiting factor [19].

Geometric considerations are also found to influence the ultimate breakdown voltage and the failure mechanism. Size of the material submitted to electrical stress [17, 19] and thickness of the dielectric [20, 21] are found to change the electrical limits. For the specific case of silicone-based dielectric elastomers, the calculated electrothermal breakdown may develop at electric fields 5-times larger than the observed breakdown field which allows to disregard this mechanism in thin structures [22]. However, it is found to contribute more significantly in multi-layered assemblies, as the dissipation of heat generated within the stack is retained [23].

Under long exposure time, partial discharges or space charge accumulation will ultimately results in failure at voltages lower than the ones obtained from short-term experiments. These time dependent phenomena contribute to the electrical ageing of the dielectric. However, the long-term performance of stretchable materials remains scarcely investigated. Studies tend to indicate a limited effect of the electrical ageing time on the mean DBS for fully relaxed polydimethylsiloxane (PDMS) membranes [19], but a faster electrical degradation under stretched conditions [24].

2.3. Mechanical limits

Elastomeric materials are widely used in various industrial applications due to their unique properties such as high elasticity, flexibility, and durability. However, these materials are prone to fatigue failure, which can significantly reduce their performance and lifespan. Fatigue failure occurs when a material is subjected to repeated mechanical loading and unloading cycles, leading to the initiation and propagation of cracks. The mechanical fatigue of elastomers is a complex phenomenon that involves various factors such as the material composition, loading pattern, and environmental conditions. The crack nucleation approach is a method used to model the fatigue behavior of elastomeric materials. This approach consists in identifying the parameters that drive the initiation of fatigue cracks in the material, such as the stress, strain, or energy-based parameters, and using this information to predict

the fatigue life of the material [25]. However, the question of determining a sole criterion for predicting elastomeric fatigue is unresolved [26]. While using the maximal principal stretch is a widely used method, it has certain drawbacks when subjected to multi-axial loadings. Studies conducted in the 80s have shown that the fatigue life is longer in simple tension than in equibiaxial tension, even when the maximum stretch value is the same [27, 28]. To tackle this limitation, the strain energy density is sometimes preferred without necessarily unifying the fatigue life obtained from different multiaxial conditions [29]. Other energy based criteria have been proposed and a parameter termed *dynamic stored energy* (DSE) provides a reliable predictor to determine the fatigue life of non-strain crystallizing elastomers submitted to uniaxial loading [30, 31]. When plotted against \log_{10} cycles to failure, this predictor was also found to linearly decrease for elastomers submitted to equibiaxial fatigue [32, 33]. In section 5.2, experimental fatigue failures are analyzed from strain and energy-based criteria to choose a suitable predictor for modeling the fatigue life of a silicone DEG.

2.4. Reliability functions

Consider a system with k independent failure mechanisms where ξ_i is the failure time of mechanism M_i with $i \in \{1, 2, \dots, k\}$. Such a system is called a series system (or a weakest link system) if its life ξ is the smallest of those potential times to failure (3) [34]

$$\xi = \min \{\xi_1, \xi_2, \dots, \xi_k\}. \quad (3)$$

In such series configuration (when the occurrence of any failure mode results in failure of the product), the system's reliability R is equal to the product of the reliability equations of the different failure modes (4)

$$R(t) = \prod R_i(t). \quad (4)$$

Experimental failure times of a particular degradation mechanism generally obeys a certain mathematical distribution which can be represented as a probability density function (*pdf*). The Weibull distribution is widely employed to

describe the life of many weakest link systems including electrical components or strength distribution of mechanical parts [35]. The general form of a 2-parameter Weibull *pdf* is given in (5) with β the shape parameter of the distribution (representing the spread in the measurement) and η the scale parameter (life at the 63.2th percentile). The reliability at time t is obtained by integrating (5) and is given in (6) for the Weibull distribution

$$f(t) = \frac{\beta}{\eta^\beta} t^{\beta-1} e^{-\left(\frac{t}{\eta}\right)^\beta} \quad (5)$$

$$R(t) = e^{-\left(\frac{t}{\eta}\right)^\beta}. \quad (6)$$

The scale parameter η which also refers to the characteristic life depends on the stress level applied (S), material parameters or design considerations. The inverse power law (IPL) (7) is widely employed, and is considered valid if the plot of the stress vs. characteristic lifetime fits a straight line on a *log-log* graph [36]. The parameter k is a constant derived from the experimental measurements and n is the ageing power exponent

$$\eta(S) = kS^{-n}. \quad (7)$$

In the next sections, the electro-mechanical reliability is obtained from mechanical and electrical characterization and the scatter observed in experimental failure is modelled with the Weibull statistic. The stress dependent lifetimes are represented using the IPL.

3. Material

The material used in this study is taken from a multi-layer assembly constituted of a stack of PDMS dielectric elastomer and electrically conductive silicone-based electrode. Both the dielectric and electrode materials are two components liquid silicone rubber obtained from a roll coating process. Further details on the material composition and samples preparation are given in [19]. The thickness of the dielectric elastomer is $145 \pm 5 \mu\text{m}$ and the thickness of the electrode is $30 \pm 5 \mu\text{m}$. To ensure a good crosslinking of the constitutive materials, a thermal post-curing is performed on the material prior to testing at a temperature of 120°C for a duration of 15 h. The dielectric silicone elastomer under evaluation in this study has a permittivity of $\varepsilon = 2.7 \times 8.85 \cdot 10^{-12} \text{ F}\cdot\text{m}^{-1}$ and a mass density of $\rho = 1130 \text{ kg}\cdot\text{m}^{-3}$, as determined through measurements.

4. Electrical reliability

In a previous work realized with the same dielectric elastomer [18], the onset of electro-mechanical instability was found to depend on the value of permittivity ε , the hyperelastic strain energy density function of the elastomer \tilde{W} , and a damage parameter D which evolves with the historical loading conditions (maximal stretch λ_{max} and number of cycles N). The damage parameter varies between 0 and 1, with 1 representing an undamaged material. The model and material parameters of [18] are re-used to determine the critical electric field E_c ,

which is identified from the maximum of the voltage to stretch function (8), where λ_3 denotes the compressive stretch in the thickness of the membrane

$$E_c = \max_{\lambda_3} \lambda_3 d_0 \sqrt{-\frac{\lambda_3 D}{\varepsilon} \frac{\partial \tilde{W}}{\partial \lambda_3}}. \quad (8)$$

In a second work [19], the breakdown strength of the same dielectric elastomer was evaluated at different ageing times and lifetime was found to obey an IPL of the applied electric field. The characteristic electric breakdown field E_t after an ageing time t_a is given in (9) with γ the power exponent of the IPL which is determined from the experimental results and t_c the ageing time required to measure E_c

$$E_t = E_c \left(\frac{t_c}{t_a} \right)^{1/\gamma}. \quad (9)$$

Considering that experimental electrical failures follow a Weibull distribution of a shape parameter β_e , and a scale parameter E_t , the electrical reliability function R_e at an electric field E is given in (10)

$$R_e = e^{-\left(\frac{E}{E_t}\right)^{\beta_e}}. \quad (10)$$

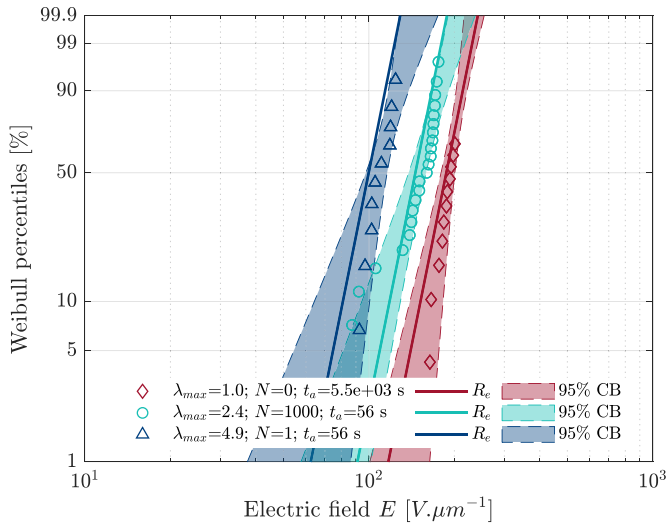
After inserting (9) into (10), the electrical reliability function R_e can be expressed as (11). As the number of cycles increases, the mechanical damage parameter progressively reduces the critical field, while the ageing time extends. This combined effect tends to diminish the system's reliability over its operational lifetime

$$R_e = e^{-\left[\left(\frac{t_a}{t_c}\right)^{1/\gamma} \left(\frac{E}{E_c}\right)\right]^{\beta_e}}. \quad (11)$$

Hence, this reliability function is derived from the material intrinsic properties on one hand, and adjusted to account for electrical ageing on the other hand. Using the model parameters given in table 2, R_e is calculated for different values of historical stretch, cycles repetitions and exposure time to electric field for a few representatives loading conditions of [18, 19]. Additionally, a more severe loading was also evaluated after stretching the film close to its mechanical limit such as covering the widest possible applicability range. Predictions of the model are compared to the experimental failures and a good agreement is obtained as R_e reasonably falls into the two-sided 95% confidence bounds of each individual failure distribution as represented by the coloured surfaces in figure 1. Accuracy of the model was also verified for more than 10 different experimental loadings and again, the different degradation mechanisms in the experimental failures were captured accurately.

Table 2. Parameters of the electrical reliability function.

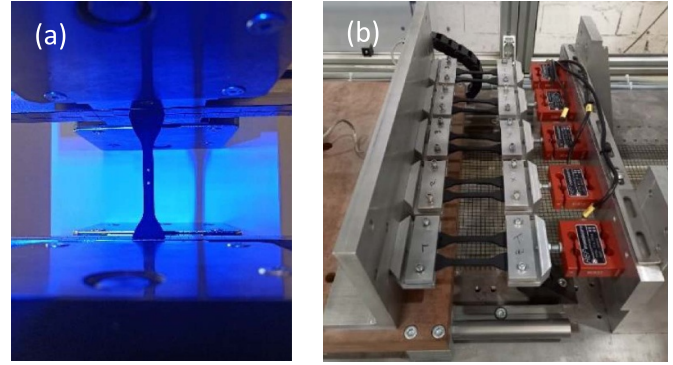
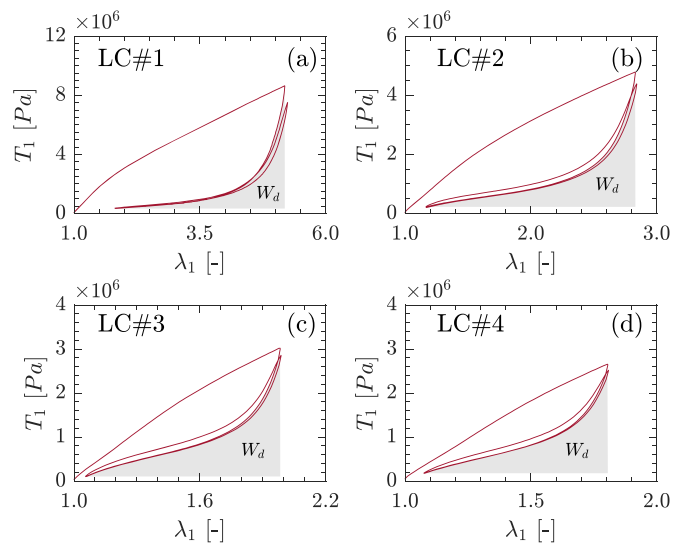
Parameter	Symbol	Value	Unit
Weibull shape parameter	β_e	10	—
Critical ageing time	t_c	56	s
IPL power exponent	γ	100	—

**Figure 1.** Experimental electrical failures (\diamond [19], \circ [18]) under different test conditions and their corresponding calculated electrical reliability function R_e .

5. Mechanical reliability

5.1. Experimental setup

First, tensile properties have been measured up to failure in uniaxial loading condition from samples prepared with a dumbbell cutter as per the geometry of ASTM D638-IV. This preliminary test is done to define the ultimate tensile properties and allows to define the upper limit from a mechanical perspective in view of the fatigue experiment. The samples were clamped in a tensile test machine (Zwick/Roell Z100) using pneumatic jaws to avoid slippage of the sample under load. The stretch in the tensile direction λ_1 is measured with a video extensometer that follows the displacement of two painted dots deposited on the sample surface (figure 2(a)). The tensile stretch is defined as $\lambda = l/l_0$ with l_0 the initial vertical distance between the two dots ($l_0 = 10$ mm) and l the evolving distance between the dots in the tensile experiment. The tensile stress T_1 is calculated using the nominal force measured by the load cell divided by the original unstretched cross-sectional area. The test is performed at a constant test speed of 50 mm min^{-1} . Following the static characterization, four different load cases (LCs) of variable severity have been evaluated in fatigue on another dynamic test bench. Tests are performed on the same dumbbell specimens used for the static characterization. Up to 10 samples can be loaded at the same elongation following a sinusoidal strain pattern at a cycling frequency of 2 Hz. Five

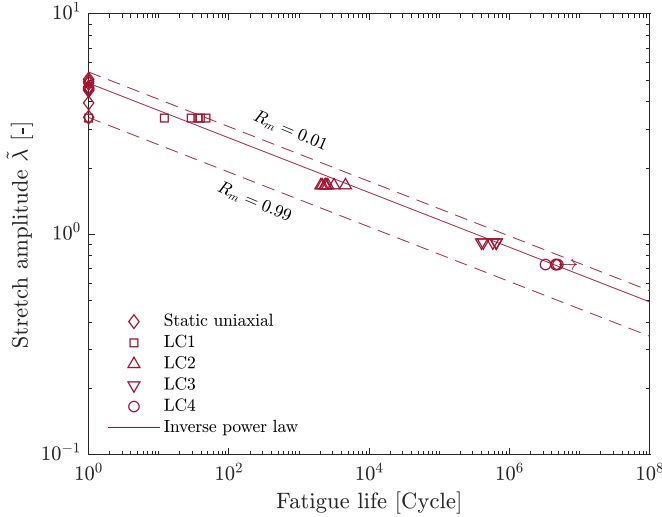
**Figure 2.** Experimental setup used for the static (a) and fatigue (b) characterization.**Figure 3.** Stress response of the first two cycles. (a) LC#1, (b) LC#2, (c) LC#3 and (d) LC#4. W_d is represented by the grey area.

load cells are connected to the static jaws and each load cell measures the tensile force applied to two samples in parallel (figure 2(b)). The fatigue test is launched until reaching failure of the whole samples. The failure is detected for each individual specimen from a sharp decrease in the recorded time-varying force signal. The video extensometer cannot be used in this fatigue setup. Therefore, the actual stretch applied for each LC was preliminary calibrated for a few cycles using the quasi-static tensile and replicating the displacement pattern applied on the fatigue machine. Results are presented in figure 3 which allows to derive the minimal and maximal stretch applied for each individual LC (table 3), and the stretch amplitude $\tilde{\lambda}$ defined as the difference between the alternating stretch extrema $\tilde{\lambda} = \lambda_{\max} - \lambda_{\min}$.

The DSE, denoted as W_d , is obtained from the area of the plot beneath the hysteresis curve where the minimum load in the cycle constitutes the lower boundary and is represented

Table 3. Test parameters of each LC.

LC	λ_{\min} [-]	λ_{\max} [-]	$\tilde{\lambda}$ [-]	W_d [$J \cdot m^{-3}$]
#1	1.82	5.19	3.37	3.80×10^6
#2	1.17	2.84	1.67	1.48×10^6
#3	1.06	1.98	0.92	7.09×10^5
#4	1.08	1.81	0.73	4.89×10^5


Figure 4. Fatigue life determined from the stretch amplitude.

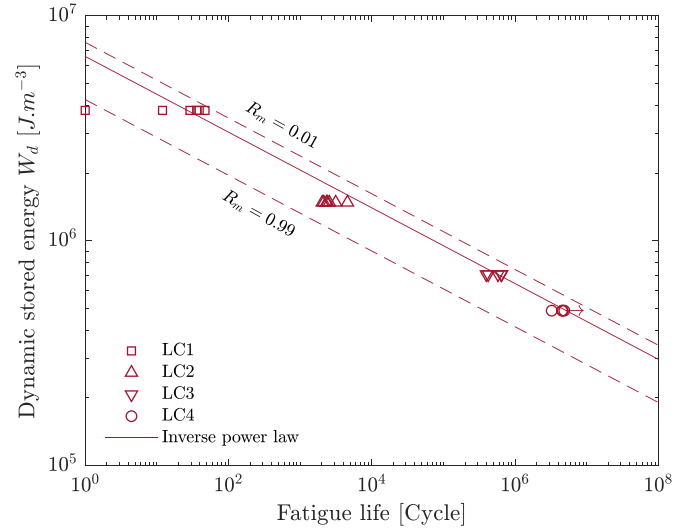
graphically by the grey area in figure 3. Its value is obtained after integrating the stress–stretch curve as defined in (12)

$$W_d = \int_{\lambda_{\min}}^{\lambda_{\max}} T_1(\lambda) d\lambda - \tilde{\lambda} T_{1\min}. \quad (12)$$

5.2. Results

Experimental fatigue failures are represented in figure 4 with the stretch amplitude $\tilde{\lambda}$ used as life predictor. The failures are represented with markers, and the suspensions (samples that have not failed) with arrows pointing to the right. For the larger amplitude (LC#1), the number of cycles to failure ranges from 1 to 47 cycles. Whereas, for the lower stretch amplitudes (LC#4) the first failure was detected after more than 3.2 million of cycles and only half of the samples were broken after stopping the experiment at more than 4.8 million cycles. The relation between the stretch amplitude and cycles to failure is linear on a \log_{10} scale and an IPL (7) is chosen for the fatigue law. The scatter in the experimental results are modelled from a Weibull distribution (5) and the resulting mechanical reliability function R_m is given in (13) with K_m and n the parameters of the IPL, β_m the shape parameter of the Weibull distribution, and N the number of cycles

$$R_m(\tilde{\lambda}, N) = e^{-(K_m \tilde{\lambda}^n N)^{\beta_m}} \quad (13)$$


Figure 5. Fatigue life determined from the dynamic stored energy density.

Experimental failures have also been analysed with the DSE as fatigue predictor (figure 5). Although a straight line on the resulting fatigue curve was obtained with this predictor, in the following, the stretch amplitude is preferred to model the mechanical fatigue life for the following reasons:

- The calculated likelihood function for the strain amplitude predictor is slightly higher than the one obtained from the DSE (table 4)
- The strain amplitude predictor can also be used to analyze the results of the static failures (which is not the case with the DSE)
- The DSE slightly decreases with the number of cycles because of a cyclic softening effect (figure 3) causing ambiguous interpretation of this predictor.

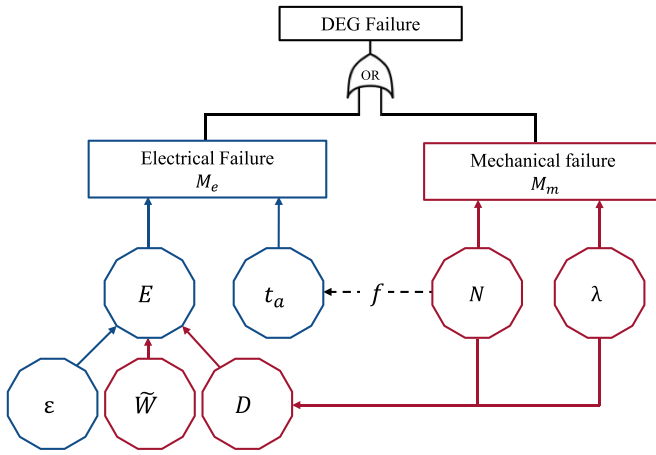
6. Electro-mechanical reliability

6.1. Model

Building a complete reliability model for a DEG given the possible large variety of degradation mechanism is extremely challenging, and a number of assumptions and simplifications need to be made. Suppose the DEG has two main independent failure mechanisms M_m and M_e , corresponding to a mechanical failure and an electrical failure respectively. In the event of a failure caused by one of these mechanisms, a DEG becomes inactive and its limited reparability results in the effective termination of its energy conversion capability. The corresponding fault tree is schematically represented in figure 6 and is used as the basis of the electro-mechanical reliability model. The stretch and number of cycles directly act on the mechanical reliability, whereas these parameters indirectly change the electrical reliability as a result of their contribution

Table 4. Parameters of the mechanical reliability function.

Parameter	Symbol	Predictor $\tilde{\lambda}$		Predictor W_d	
		Value	Unit	Value	Unit
Weibull shape	β_m	1.6	—	1.8	—
IPL constant	K_m	3.0×10^{-6}	—	3.1×10^{-41}	$[\text{J} \cdot \text{m}^{-3}]^{-n}$
IPL Power exponent	n	8.1	—	5.9	—
Calculated likelihood function		-161	—	-209	—

**Figure 6.** Fault tree of the DEG used in the electro-mechanical reliability model (arrows indicating interactions between the parameters).

to the mechanical damage parameter. Inserting the reliability functions of these two failure mechanisms into (4) yields to the electro-mechanical reliability function R_{em} given in (14). In the following, the mechanical reliability function R_m is obtained from (13) whereas the electrical reliability function R_e is defined according to (11)

$$R_{em} = R_e R_m \quad (14)$$

In the electro-mechanical reliability function, t_a represents the ageing time at maximal electric field. However, for the harvesting cycles presented in table 1, the electric field varies throughout the cycle duration. This variation requires the determination of an equivalent ageing time \tilde{t}_a (15), using the IPL, where T denotes the period of one mechanical cycle. Consider a CE cycle where the stretch is a sinusoidal function of time. In this scenario, the electric field reaches and maintains its maximum value for half of the cycle's period. Consequently, the equivalent electrical aging time simplifies to $\tilde{t}_a = N/2f$, with f the mechanical frequency at which the DEG operates

$$\tilde{t}_a = \frac{N}{E_{\max}^\gamma} \int_0^T E(t)^\gamma dt. \quad (15)$$

6.2. Application

Assume a silicone based DEG composed of the materials described in previous sections and submitted to a constant, sinusoidal stretch at a cycling frequency of $f = 1$ Hz. Under equibiaxial loading, the capacitance swing is equal to $\hat{\beta} = (\lambda_{\max}/\lambda_{\min})^4$. This relation is used in the energy density equations presented in table 1 where λ_{\min} is defined at the onset of loss of tension (when the stress in the direction the applied mechanical stretch reaches zero in the relaxing phase). From an energetic perspective, it is essential to maximize both the applied maximal electric field and the maximal stretch. But, from a reliability standpoint the probability of failure $U_{em} = 1 - R_{em}$ also rises with increasing values of λ_{\max} and E_{\max} as represented in figure 7 for a first harvesting cycle. The iso-reliability lines can be decomposed into distinct phases: a first reduction in the maximal electric field caused by the Mullins damage, and a second region where the reliability lines become vertical once the ultimate tensile stretch is reached. For the highest theoretical energy densities reported in literature, the reduction in DBS associated to mechanical damage is ignored [2]. For the silicone evaluated here, the ultimate stretch and dielectric breakdown determined independently are represented by the dashed lines in figure 7, resulting in a theoretical energy density of $3.4 \text{ J} \cdot \text{g}^{-1}$ (for a CE cycle). But this approach falls into a region of extremely high unreliability (at the location of the star marker in figure 7), highlighting the critical importance of accounting for the detrimental effect of the mechanical damage when evaluating the energy density.

When the number of mechanical cycles increases, the iso-reliability lines are significantly shifted towards lower λ_{\max} values as represented in figure 8 as the influence of mechanical fatigue becomes predominant in the overall reliability balance. The reliability lines are also shifted to lower values of electric field because of the combined effect of electrical ageing and cycle softening. However, this second degradation remains marginal in comparison of the one resulting from the mechanical fatigue.

6.3. Levelized energy density

As suggested by Jean-Mistral one should aim to maximize the energy conversion over the system's lifetime [12]. We introduce here a new metric \bar{w}_e which takes up this concept while considering the electro-mechanical reliability in the conversion efficiency of the DEG (16). It basically represents

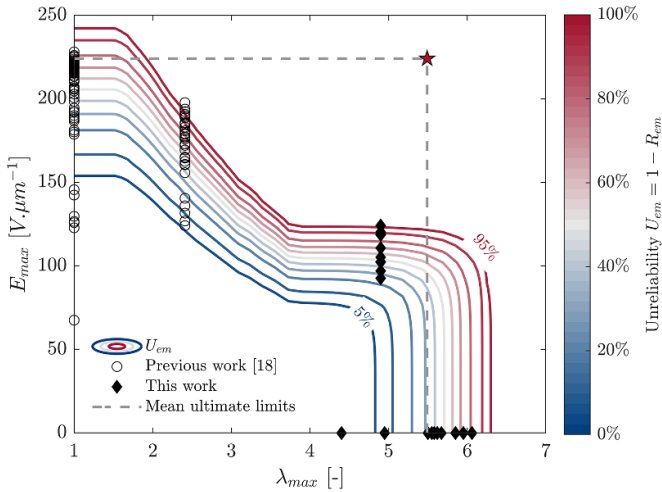


Figure 7. Electro-mechanical unreliability of the first harvesting cycle ($N = 1$).

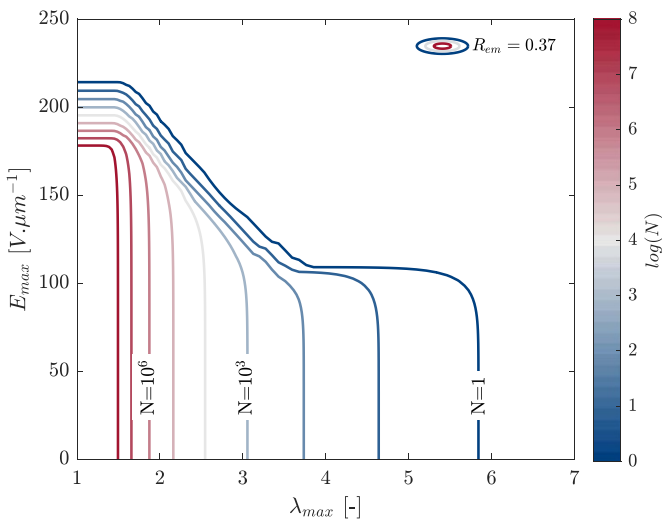


Figure 8. Evolution of the iso-reliability line ($R_e = 0.37$) with cycling.

the energy density weighed by the value of the reliability after an operating time T . The full derivation of this metric is detailed in the [appendix](#) and its value calculated using a numerical integration technique at different lifetimes for a range of operating conditions (λ_{\max} and E_{\max}). This index \bar{w}_e is hereafter defined as the *levelized energy density*

$$\bar{w}_e = \frac{w_e}{T} \int_0^T R_{em}(t) dt. \quad (16)$$

It is of interest to analyze this metric in a stretch vs. electric field diagram as the value of \bar{w}_e shows a maximum $\hat{w}_e = \max(\bar{w}_e)$ which evolves as the design life of a DEG increases as represented in figure 9 for a CE cycle. This maximum gives the optimal operating parameters (denoted λ_{opt} and E_{opt}) which maximize the energy conversion over the period considered. In other words, a DEG operated away from this maximum in figure 9 would be less efficient either because

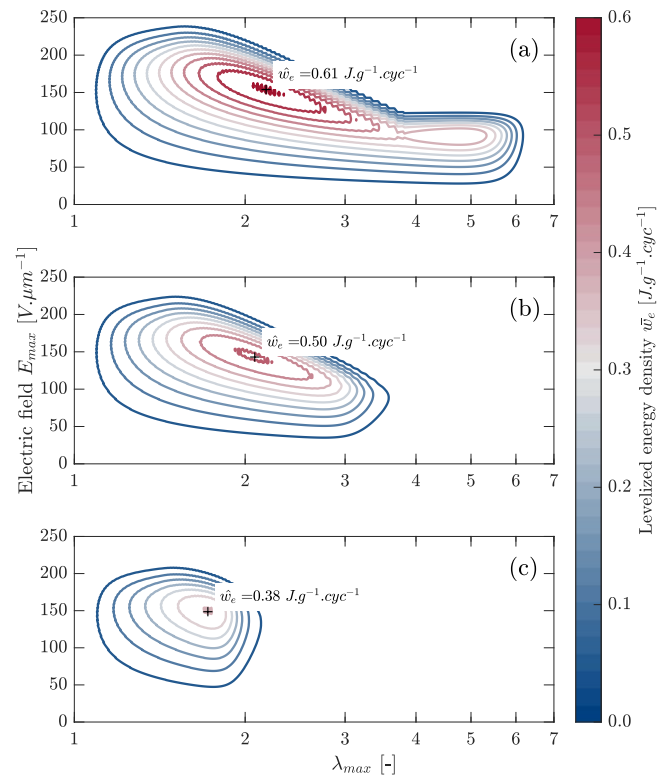


Figure 9. Levelized energy density of the CE cycle for a design lifetime of 1 cycle (a), 1000 cycles (b) and 1 million cycles (c).

the energy conversion per cycle is too low (bottom left of the diagram) or because the DEG would be too unreliable and prone to premature failure (top right of the diagram). For a DEG aimed to be used only for one CE cycle, the optimal stretch is $\lambda_{\text{opt}} = 2.3$ and the optimal maximal electric field is $E_{\text{opt}} = 154 \text{ V} \cdot \mu\text{m}^{-1}$ (figure 9(a)). This yields to an energy density of $0.61 \text{ J} \cdot \text{g}^{-1}$ which is aligned with the highest energy densities reported for DEG realized on a limited number of cycles (although these results were obtained with different material systems and different harvesting strategies) [4, 37].

The same methodology has been applied to the OT and CC cycles. In these cases, the *levelized energy density* differs from that of the CE cycle due to two main factors: a different energy density equation and a lower electrical aging time (as the DE is exposed to the maximal electric field for shorter durations). These variations result in different optimal operating parameters. The optimal stretch is notably reduced for the CC cycles ($\lambda_{\text{opt}} = 1.88$), while higher optimal field cycles are calculated.

Surprisingly, for the three harvesting cycles evaluated, the optimal stretch is significantly lower than the mean ultimate stretch measured in the tensile experiment ($\lambda_{\max} = 5.5$). This reduction is attributed to the Mullins softening in the elastomer which significantly reduces the DBS. After a first cycle up to $\lambda_{\max} = 4.9$, the mean experimental breakdown strength is $109 \pm 7 \text{ V} \cdot \mu\text{m}^{-1}$ representing only 49% of the value measured on a sample that was never stretched. Because of the quadratic contribution of E_{\max} to the energy density, it is therefore

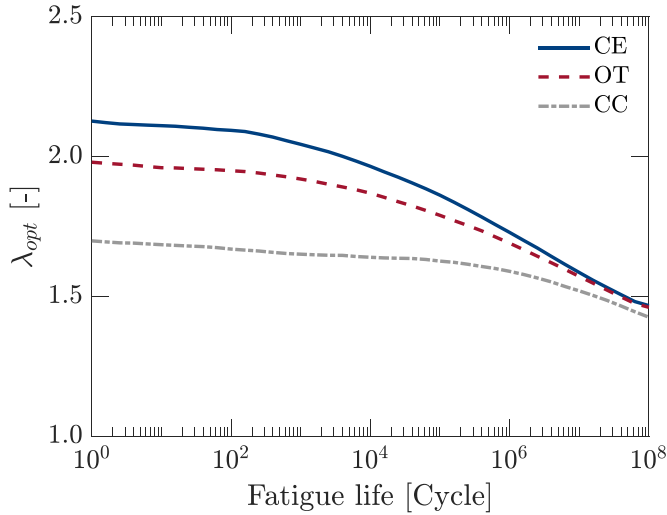


Figure 10. Optimal maximal stretch.

preferable to limit the stretch such as limiting the DBS degradation and it explains why the optimal stretch is calculated at only a fraction of the intrinsic mechanical limit. Consequently, the *levelized energy density* after one cycle is more than 5-fold lower than the energy density calculated from the mean static failures measured if ultimate electrical and mechanical limits are determined independently.

In the high cycle domain, the difference in optimal parameters between the various harvesting schemes tends to fade away. For a system aimed to be used for 1 million of cycles, the optimal stretch reduces to $\lambda_{\max} = 1.7$ for both the CE and OT cycle and down to $\lambda_{\max} = 1.6$ for the CC cycle (figure 10). The optimal electric field is however relatively insensitive to cycling and the small variations are attributed to two competing mechanisms having opposite contributions to the critical field (figure 11). On one hand, the degradation resulting from multiple cycles and long ageing times tends to reduce the operating field, but on the other hand, when the design life increases, the optimal stretch is also smaller leading to a reduced Mullins damage. The convergence of optimal parameters observed in the fatigue domain has significant implications on the levelized energy density. As illustrated in figure 12, the difference in energy density between CE and OT cycles becomes negligible beyond 1 million cycles. This convergence emphasizes the preferential selection of the OT cycle due to its simplified electronic architecture.

While this study contributes valuable insights into the long-term performance of DEG under combined electrical and mechanical stress, several areas require further investigations. Our findings will have to be verified under more representative operating conditions where the voltage and stretch are varying continuously and simultaneously. In future work, we will upgrade our fatigue test bench in order to replicate the constant-field cycle for providing a more robust understanding of the electro-mechanical degradation mechanisms. Additionally, the question of mechanical fatigue under multi-axial loading conditions remains to be further investigated as the capacitance swing and the resulting energy

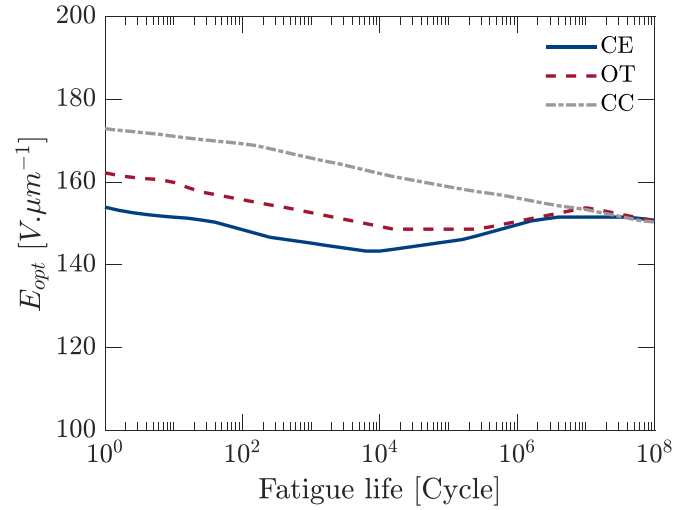


Figure 11. Optimal maximal electric field.

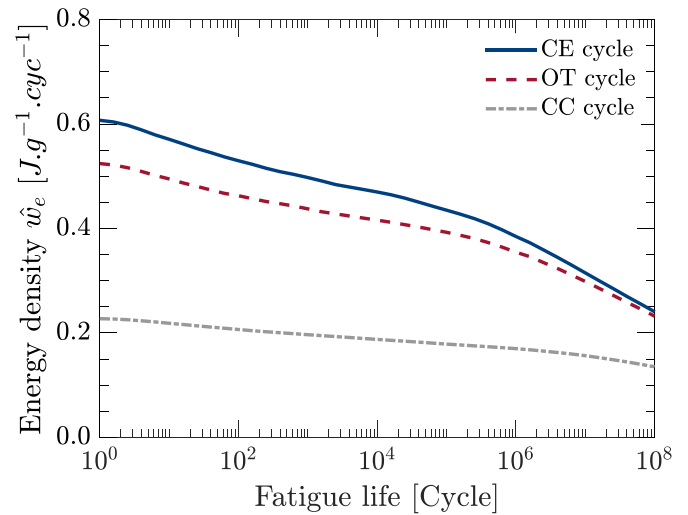


Figure 12. Maximal levelized energy density of the different harvesting cycles.

conversion are maximized when the dielectric membrane is stretched along multiple directions.

7. Conclusion

This study proposes an innovative electrical reliability model that accounts for the combined effects of mechanical damage and electrical ageing in dielectric elastomers. The model is developed through a comprehensive approach involving both experimental and theoretical components. Separately, mechanical fatigue experiments were conducted on a silicone-based dielectric elastomer. The results revealed that the stretch amplitude serves as a reliable predictor for determining the fatigue life of the material. The reliability functions of the individual failure mechanisms (namely mechanical and electrical failures) were combined into a series model, and the resulting electro-mechanical reliability model accurately captures the

experimental failures observed under a wide range of test conditions. Outcome of this model is used in a novel energy metric termed *levelized energy density* which considers the role of the electro-mechanical degradation in the conversion efficiency of a DEG. The methodology has been applied to the CE, OT and CC cycles and enables the derivation of optimal stretch and electric field values, with the objective of maximizing the cumulative energy converted over the design life of the DEG transducer. The proposed electro-mechanical reliability model, coupled with the levelized energy density metric, provides a comprehensive framework for understanding and optimizing the performance of dielectric elastomer-based energy conversion systems. This approach accounts for the interplay between mechanical and electrical degradation mechanisms, enabling more accurate predictions and informed design decisions.

Mechanical fatigue is often disregarded in the performance evaluation of dielectric elastomers. Our analysis suggests that it plays a major contribution in the overall energy balance of a silicone-based DEG. Estimating the energy density from the mean static mechanical and electrical limits is found to be unrealistic, and our analysis shows a value at least 5 times lower after a first CE cycle realized under optimal stretch and electric field conditions. An additional 38% decrease in the energy density is expected for a design life of 1 million cycles. The main causes of these reductions are first the Mullins damage which reduces the operating electric field, and secondly the depletion needed in the stretch amplitude for ensuring the mechanical integrity of the DEG.

These findings were obtained under non-concomitant electrical and mechanical degradation and therefore likely give the upper theoretical limits. Further work with combined electrical and mechanical stresses will be required to better assess the real potential of DEG as long-lasting transducers.

Data availability statement

All data that support the findings of this study are included within the article (and any supplementary files).

Acknowledgment

This work was supported by SBM Offshore in the framework of the S3[®] Wave Energy Converter development.

Appendix. Derivation of the levelized energy density

Assuming a system composed of k_0 independent DEG, submitted to the same mechanical loading at a constant cycling frequency f . The initial power P_0 of such system considering the entire DEGs are initially functional equals to (17) with Ω the active volume of dielectric contained in a DEG

$$P_0 = k_0 f \Omega \rho w_e. \quad (17)$$

After some time in operation and a subsequent number of cycles, a fraction of the DEG becomes inactive because of a

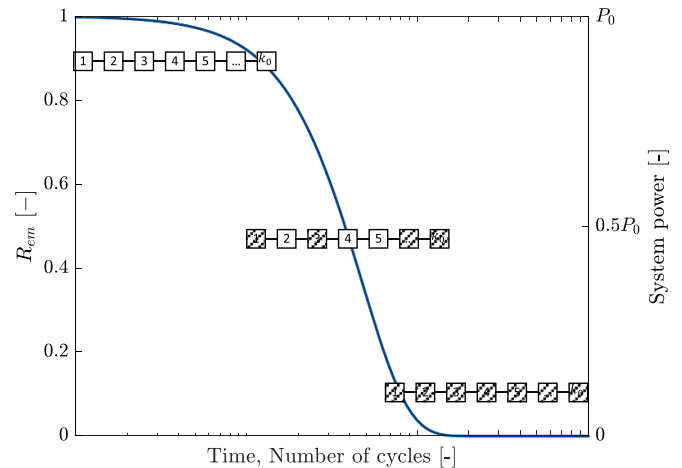


Figure 13. An example of a time-evolving electro-mechanical reliability function and the corresponding illustration of the ratio of active DEGs.

mechanical failure or an electrical breakdown. Consequently, only k operational DEG (out of the k_0 initially composing the system) are contributing to the overall power P of the system. When the DEG population is sufficiently large, the fraction of active generators k/k_0 equals the value of the electro-mechanical reliability function, which yields to (18)

$$P(t) = P_0 \frac{k(t)}{k_0} \approx P_0 R_{em}(t). \quad (18)$$

Ultimately, the entire DEGs may become inactive resulting in a null power of the system when the lifetime tends to infinity as illustrated in figure 13. The cumulated energy U_c converted by the system after a time T is obtained by integrating (18)

$$U_c = P_0 \int_0^T R_{em}(t) dt \quad (19)$$

The *levelized energy density* is obtained after dividing the cumulated energy by the entire mass of dielectric material initially composing the system, and the number of mechanical cycles completed (20)

$$\bar{w}_e = \frac{U_c}{N k_0 \rho \Omega}. \quad (20)$$

After substituting U_c with (19), and P_0 with (17), it yields to (21) for the equation of the *levelized energy density* used in section 6.3

$$\bar{w}_e = \frac{w_e}{T} \int_0^T R_{em}(t) dt \quad (21)$$

ORCID iDs

Emmanuel Taine <https://orcid.org/0000-0002-9591-7203>
Thomas Andritsch <https://orcid.org/0000-0002-3462-022X>

References

- [1] Koh S J A, Keplinger C, Li T, Bauer S and Suo Z 2011 Dielectric elastomer generators: how much energy can be converted? *IEEE/ASME Trans. Mechatronics* **16** 33–41
- [2] Koh S J A, Zhao X and Suo Z 2009 Maximal energy that can be converted by a dielectric elastomer generator *Appl. Phys. Lett.* **94** 262902
- [3] Jean-Mistral C, Basrouf S and Chaillout J-J 2010 Modelling of dielectric polymers for energy scavenging applications *Smart Mater. Struct.* **19** 105006
- [4] Shian S, Huang J, Zhu S and Clarke D R 2014 Optimizing the electrical energy conversion cycle of dielectric elastomer generators *Adv. Mater.* **26** 6617–21
- [5] Rosset S and Anderson I A 2022 Squeezing more juice out of dielectric elastomer generators *Front. Robot. AI* **9** 825148 (in English)
- [6] Moretti G, Rosset S, Vertechy R, Anderson I and Fontana M 2020 A review of dielectric elastomer generator systems *Adv. Intell. Syst.* **2** 2000125
- [7] Xu Z et al 2023 Fatigue-resistant high-performance dielectric elastomer generator in alternating current method *Nano Energy* **109** 108314
- [8] Chiba S, Waki M, Kornbluh R and Pelrine R 2011 Current status and future prospects of power generators using dielectric elastomers *Smart Mater. Struct.* **20** 124006
- [9] Moretti G, Righi M, Vertechy R and Fontana M 2017 Fabrication and test of an inflated circular diaphragm dielectric elastomer generator based on PDMS rubber composite *Polymers* **9** 283
- [10] Zhou J, Jiang L and Khayat R E 2015 Investigation on the performance of a viscoelastic dielectric elastomer membrane generator *Soft Matter* **11** 2983–92
- [11] Zhou J and Jiang L 2018 Development of a predictor for fatigue crack nucleation of dielectric viscoelastomers under electromechanical loads *J. Mech. Phys. Solids* **119** 400–16
- [12] Jean-Mistral C, Jacquet-Richardet G and Sylvestre A 2020 Parameters influencing fatigue life prediction of dielectric elastomer generators *Polym. Test.* **81** 106198
- [13] Li W, Liu X, Jiang Y, Wu W, Yu B, Ning N, Tian M and Zhang L 2022 Extremely high energy density and long fatigue life of nano-silica/polymethylvinylsiloxane dielectric elastomer generator by interfacial design *Nano Energy* **104** 107969
- [14] Vudayagiri S, Zakaria S, Yu L, Hassouneh S, Benslimane M and Skov A 2014 High breakdown-strength composites from liquid silicone rubbers *Smart Mater. Struct.* **23** 105017
- [15] Kollosche M and Kofod G 2010 Electrical failure in blends of chemically identical, soft thermoplastic elastomers with different elastic stiffness *Appl. Phys. Lett.* **96** 071904
- [16] Kofod G, Sommer-Larsen P, Kornbluh R D and Pelrine R 2003 Actuation response of polyacrylate dielectric elastomers *J. Intell. Mater. Syst. Struct.* **14** 787–93
- [17] Zakaria S, Morshuis P H F, Benslimane M Y, Yu L and Skov A L 2015 The electrical breakdown strength of pre-stretched elastomers, with and without sample volume conservation *Smart Mater. Struct.* **24** 055009
- [18] Taine E, Andritsch T, Saeedi I A and Morshuis P H F 2023 Dielectric breakdown strength of PDMS elastomers after mechanical cycling *Energies* **16** 7424
- [19] Taine E, Andritsch T, Saeedi I A and Morshuis P H F 2023 Size effect and electrical ageing of PDMS dielectric elastomer with competing failure modes *Smart Mater. Struct.* **32** 105021
- [20] Huang J, Shian S, Diebold R M, Suo Z and Clarke D R 2012 The thickness and stretch dependence of the electrical breakdown strength of an acrylic dielectric elastomer *Appl. Phys. Lett.* **101** 122905
- [21] Gatti D, Haus H, Matysek M, Frohnapfel B, Tropea C and Schlaak H F 2014 The dielectric breakdown limit of silicone dielectric elastomer actuators *Appl. Phys. Lett.* **104** 052905
- [22] Zakaria S, Morshuis P, Benslimane M, Gernaey K and Skov A 2014 The electrical breakdown of thin dielectric elastomers: thermal effects *Proc. SPIE* **9056** 90562V
- [23] Christensen L R, Hassager O and Skov A L 2019 Electro-thermal model of thermal breakdown in multilayered dielectric elastomers *AIChE J.* **65** 859–64
- [24] Iannarelli A, Niasar M G and Ross R 2019 The effects of static pre-stretching on the short and long-term reliability of dielectric elastomer actuators *Smart Mater. Struct.* **28** 125014
- [25] Mars W V and Fatemi A 2004 A literature survey on fatigue analysis approaches for rubbers *Int. J. Fatigue* **24** 949–61
- [26] Abraham F, Alshuth T and Jerrams S 2005 The effect of minimum stress and stress amplitude on the fatigue life of non strain crystallising elastomers *Mater. Des.* **26** 239–45
- [27] Roberts B and Benzies J 1977 The relationship between uniaxial and equibiaxial fatigue in gum and carbon black filled vulcanizates *Proc. Rubbercon* vol 77 pp 1–13
- [28] Roach J F 1982 *Crack Growth in Elastomers under Biaxial Stresses* (The University of Akron)
- [29] Mars W and Fatemi A 2004 Factors that affect the fatigue life of rubber: a literature survey *Rubber Chem. Technol.* **77** 391–412
- [30] Abraham F 2002 *The Influence of Minimum Stress on the Fatigue Life of Non Strain Crystallising Elastomers* (Coventry University)
- [31] Alshuth T, Abraham F and Jerrams S 2002 Parameter dependence and prediction of fatigue properties of elastomer products *Rubber Chem. Technol.* **75** 635–42
- [32] Zhou Y, Jerrams S, Betts A and Chen L 2014 Fatigue life prediction of magnetorheological elastomers subjected to dynamic equi-biaxial cyclic loading *Mater. Chem. Phys.* **146** 487–92
- [33] Jerrams S, Hanley J, Murphy N and Ali H 2008 Equi-biaxial fatigue of elastomers: the effect of oil swelling on fatigue life *Rubber Chem. Technol.* **81** 638–49
- [34] Chen Y, Yang L, Ye C and Kang R 2015 Failure mechanism dependence and reliability evaluation of non-repairable system *Reliab. Eng. Syst. Saf.* **138** 273–83
- [35] Weibull W 1952 A statistical distribution function of wide applicability *J. Appl. Mech.* **18** 293–7
- [36] Feilte E A 2018 Lifetime assessment of electrical insulation *Electric Field* (IntechOpen)
- [37] Huang J, Shian S, Suo Z and Clarke D R 2013 Maximizing the energy density of dielectric elastomer generators using equi-biaxial loading *Adv. Funct. Mater.* **23** 5056–61